

# Electrochromic Device Response Controlled by an *In-situ* Polymerized Ionic Liquid Based Gel Electrolyte

Rambabu Sydam<sup>a</sup>, M. Deepa<sup>a,\*</sup>, A.K. Srivastava<sup>b</sup>

<sup>a</sup>*Department of Chemistry, Indian Institute of Technology Hyderabad,*

*Yeddumailaram-502205, Andhra Pradesh, India*

<sup>b</sup>*National Physical Laboratory, Dr. K.S. Krishnan road, New Delhi-11001, India*

## Abstract

Polymer electrolytes were synthesized by two different approaches and applied to electrochromic devices based on electrodeposited tungsten oxide (WO<sub>3</sub>) or Poly(3,4-ethylenedioxythiophene) (PEDOT) films as cathodes, and a Prussian Blue (PB) film as anode. The first method involved the entrapping of an ionic liquid in a polymer host (poly(methylmethacrylate) or PMMA) and the second approach relied on the *in-situ* thermal polymerization of methylmethacrylate (MMA) in the hydrophobic ionic liquid, yielding a solidified transparent gel. The effect of *in-situ* solid polymer electrolyte formation on device performance characteristics was realized in terms of a larger coloration efficiency of 119 cm<sup>2</sup> C<sup>-1</sup> ( $\lambda = 550$  nm) achieved for the WO<sub>3</sub>-PB (MMA) device as compared to a value of 54 cm<sup>2</sup> C<sup>-1</sup> obtained for the WO<sub>3</sub>-PB (PMMA) device. Similar enhancements in electrochromic coloring efficiency, reflectance contrast, and faster switching kinetics were obtained for the PEDOT-PB (MMA) device. The strategy of introducing an electrolyte to the electrochromic device in a liquid state and then subjecting the same to gradual polymerization allows greater accessibility of the electrolyte ions to the active sites on the electrochromic electrodes and superior interfacial contact. As a consequence, larger optical contrast and faster kinetics are achieved in the MMA based devices. While PEDOT films were amorphous, PB films were semi-crystalline but only in case of WO<sub>3</sub>, the hexagonal structure of

WO<sub>3</sub>, equipped with three/four/six-coordinated voids was found to affect bleaching kinetics favorably. The performance of PMMA based electrolyte is limited by high resistance at the electrode/electrolyte interface, and a lesser number of ions available for oxidation and reduction. Large area (~10 cm × 4 cm) devices were also fabricated using this simple wet chemistry method and their ability to color uniformly without any pinholes was demonstrated.

*Keywords:* Tungsten oxide; Poly(3,4-ethylenedioxythiophene); Prussian Blue; electrochromic devices; polymer electrolyte

## **1. Introduction**

Electrochromic windows, by dynamically controlling the amount of light and solar energy that can pass through the device, help save energy in buildings and automobiles.<sup>1-3</sup> They consist of two complementary coloring electrochromic layers that change optical properties persistently and reversibly when an electrical voltage is applied. An ion conducting electrolyte separates the two coatings and together the layers and the electrolyte allow the transport of electrons and ions. One layer acts as a positive electrode (e.g. Prussian blue) and another layer (e.g. tungsten oxide) serves as a negative electrode. When voltage is applied, cations stored in the positive electrode, traverse to the negative electrode, a phenomenon that converts transparent tungsten oxide to a tungsten metal bronze (a light absorbing – blue layer) formed by the electrochemical intercalation of ions. Concurrently, the anodic Prussian blue layer undergoes oxidation and attains a deep blue color, which is complementary to the color change experienced by the cathodic tungsten oxide film. The longer the period, for which the bias is applied, more ions are inserted and the device becomes darker.<sup>4,5</sup>

On reversing the applied voltage, the process is also reversed. These devices require a very low dc voltage (~ 1.0 - 3.0 V) and only use energy to change their optical state, not maintain any particular state. Typically, response times vary from a few seconds to a few minutes

depending upon the size of the device. The technology can thus save substantial amounts of energy in buildings and automobiles. Among various solar control windows which are commercially available today, such as suspended particle devices, photochromic, thermochromic, tinted and reflective glass, electrochromic windows are the ones which offer the best compromise between electric lighting and cooling energy.<sup>3-5</sup>

The challenge in electrochromic devices is therefore to develop low cost processes and components to enable fabrication of devices capable of delivering high contrast ratios and long term durability. Tungsten oxide and poly(3,4-ethylenedioxythiophene) or PEDOT find widespread application as cathodically coloring electrodes in electrochromic smart windows, dynamic displays, eyewear and variable reflectance devices like mirrors.<sup>6-9</sup> The ability of tungsten oxide to sustain tens of thousands of repetitive cycles of coloration and bleaching, high optical transparency in the visible and infrared regions, in the fully oxidized state, good UV and chemical stability, render it as an efficient electrode in electrochromic devices.<sup>3,4</sup> Similarly, PEDOT films offer stable color switching between light transmissive blue and deep blue colors, are cost effective, have a moderately low band gap in the range of 1.5 to 1.6 eV and possess large electronic conductivity in the doped form, thus enabling their use as electrochromic electrodes in smart windows.<sup>10,11</sup> Prussian Blue (PB) is an ideal choice for the counter electrode, as it undergoes a complementary color switch between Prussian white ( $[\text{Fe}^{\text{II}}\text{Fe}^{\text{II}}(\text{CN})_6]^{2-}$ , Everitt's salt) which, appears as a thin transparent film and is formed upon electrochemical reduction of Prussian Blue ( $[\text{Fe}^{\text{III}}\text{Fe}^{\text{II}}(\text{CN})_6]^-$ , PB).<sup>12</sup> The electrolyte or the ion conducting medium is also an important component of the device and the use of solid polymer electrolytes aids in the formation of leakage free laminated devices. In the past, a few reports have either focused largely on the properties of polymer electrolytes or evaluated the electrochromic response of electrochromic devices or films,<sup>13-20</sup> but a combination of the electrolyte properties and how it

affects the darkening/bleaching phenomena in electrochromic devices is relatively less investigated.

Among various studies on electrochromic devices, one report on display devices of small dimensions based on thin walled nanotubes of PEDOT, is particularly noteworthy, as the devices showed very fast switching times of about 10 ms.<sup>21</sup> Another study of significance focused on the formation of PEDOT/Poly(aniline) devices wherein the electrodes were fabricated using a layer-by-layer assembly and bleaching times of the order of sub-seconds were attained, but the dimensions of the device were not large.<sup>22</sup> In a recent study, PEDOT/PB devices of  $12 \times 15 \text{ cm}^2$  dimensions containing an ionic liquid based gel electrolyte were fabricated using flexible substrates.<sup>23</sup> Yet another report that must be mentioned stressed on devices wherein polyester-based foils were used as substrates, one was coated with a tungsten oxide film colored by sputtering in the presence of  $\text{H}_2$  and another with a nickel-vanadium oxide film colored by post-deposition ozone exposure.<sup>3</sup> These films were laminated together by a poly(methyl methacrylate) or PMMA-based electrolyte and the devices were able to endure 5000 color-bleach cycles, without undergoing any significant loss in color contrast.<sup>3</sup> In the past, we have also investigated electrochromism and electrochemistry of PEDOT based cells containing poly(vinyl alcohol) based on free standing electrolyte films and of about  $5 \times 5 \text{ cm}^2$  dimensions.<sup>24,25</sup>

Despite sustained efforts in the area of fabrication and characterization of electrochromic devices, a systematic study on how the procedure used for electrolyte application to a device influences the electrochromic behavior of the ensuing devices remains unreported to date. Further, there are concerns regarding the dissolution of electrode materials in electrolyte used in devices, the adverse effects of oxygen and water vapor infusion, and degradation at surfaces and interfaces. Since all the above said factors limit durability, it is therefore imperative to identify electrolytes and device fabrication procedures that will not deteriorate the electrochromic performance when subjected to practical use for the desired operational lifetime of the device.

Keeping these aspects in view, in the present report, we fabricated electrochromic devices based on PEDOT-PB and WO<sub>3</sub>-PB and used two different approaches for synthesizing a polymer electrolyte based on a hydrophobic ionic liquid and applying the same to these devices. We preferred a pyrrolidinium ion based ionic liquid, as due to its' non-aromatic character (in comparison to an imidazolium ion), the pyrrolidinium electrolyte is known to be electrochemically more stable than the imidazolium electrolyte and is therefore more suitable for electrochromic or electrochemical devices.<sup>26,27</sup> The first method involved the direct application of a gel polymeric electrolyte to a cavity created by a spacer on the electrochromic electrode and sealing. In the second approach, the electrolyte containing the monomer is injected into a pre-sealed electrochromic device in liquid state and subjected to *in-situ* thermal polymerization, to bring about the solidification of the electrolyte solution. The comparison of electrochromic performance characteristics of PEDOT-PB and WO<sub>3</sub>-PB devices based on the *in-situ* polymerized gel electrolyte *versus* a conventional polymeric electrolyte showed dramatic differences in terms of absorbance / reflectance modulation, coloration efficiency, redox response, color-bleach kinetics and charge transport characteristics. Despite the complexity of the comparison, owing to the multiple components of the device, our study attempts to provide an understanding of how the electrolyte incorporation method can alter the electrochromic response of the devices.

## 2. Experimental

### 2.1. Materials

Tungsten (W) metal powder (< 100 μm), Potassium ferricyanide (K<sub>3</sub>[Fe(CN)<sub>6</sub>]), ferric chloride (FeCl<sub>3</sub>), Polyethylene glycol 400 (PEG), 1-butyl-1-methyl pyrrolidinium bis(trifluoromethylsulfonyl)imide, **Benzoyl peroxide (with 25% H<sub>2</sub>O)** and reagents: acetone, HCl, methanol, isopropanol, hydrogen peroxide (H<sub>2</sub>O<sub>2</sub>, 30 %) of GR/AR grade were obtained

from Merck and used as received. Methylmethacrylate (MMA), Camphorsulfonic acid (CSA), 3,4-ethylenedioxythiophene (EDOT) and Poly(methylmethacrylate) (PMMA, M.W. = 996000) were procured from Sigma Aldrich. Ultrapure water (resistivity~ 18.2 MΩ cm) obtained through Millipore Direct-Q 3 UV system was used as solvent.

## 2.2. Synthesis of Electrochromic Films

Tungsten (W) metal powder (13.0 g) was dissolved in 80 mL of H<sub>2</sub>O<sub>2</sub> at ~50–60 °C and decomposition of excess peroxide was accomplished by refluxing at the same temperature for 2–3 hours. To the resulting turbid solution, 8 mL of PEG and 30 mL of iso-propanol were added which, was followed by filtration to yield a clear yellow precursor solution. Potentiostatic electrodeposition was performed in a three electrode electrochemical cell with a platinum sheet as the auxiliary electrode, a SnO<sub>2</sub>:F coated glass substrate as the working electrode and the reference electrode was Ag/AgCl/KCl. A constant potential of –1.2 V was applied for five minutes, and a blue colored film was formed on the working electrode. The SnO<sub>2</sub>:F coated glass substrates procured from Pilkington were 4 mm thick, had a sheet resistance of 14 Ω/sq. The films were transparent; these were rinsed in deionized water and dried in air. Dissolution of 0.1 M of EDOT, 0.1 M LiCF<sub>3</sub>SO<sub>3</sub>, 1.2 M camphorsulfonic acid (CSA) in 15 mL of deionized water and 10 mL of isopropanol resulted in a colorless solution. The solution was magnetically stirred for thirty minutes at room temperature. The clear sol was used for the oxidative electropolymerization of EDOT onto transparent conducting SnO<sub>2</sub>:F coated glass substrates under potentiostatic conditions (+1.2 V), in a three electrode system with another SnO<sub>2</sub>:F coated glass substrate as counter electrode and Ag/AgCl/KCl as reference electrode, for three minutes. Films were rinsed in methanol and stored in air. Prussian blue films were grown from a solution of 10 mM K<sub>3</sub>[Fe(CN)<sub>6</sub>] and 10 mM FeCl<sub>3</sub> in 0.01 N HCl in a three electrode electrochemical cell using Ag/AgCl/KCl as reference electrode by applying a fixed potential of +1.5 V for 300 s to a

SnO<sub>2</sub>:F coated glass substrate. Films were washed in a solution of 0.01 N HCl and deionized water mixed in a 2:3 volume ratio and stored in air.

### 2.3. Synthesis of Electrolytes and Devices

In the first approach, an acrylic adhesive tape (640 μm thick and 3 mm wide) was applied along the four edges of the glass on the cathodically coloring electrode (WO<sub>3</sub> or PEDOT) and the complementary electrode (PB) was then placed above this electrode and two 1 mm wide openings were grafted in the tape along one edge. Except for the two openings, the remainder of this assembly was sealed with an epoxy. MMA was passed through an activated neutral alumina column, to remove the inhibitor. To the ionic liquid: 1-butyl-1-methyl pyrrolidinium bis(trifluoromethylsulfonyl)imide, 30 wt. % of MMA was added and benzoyl peroxide (1 wt. % relative to MMA) was used as an initiator. The electrolyte injected using a glass syringe through one of the open ports in the device, and the device was then placed vertically in an oven for *in-situ* thermal polymerization at 60-70 °C for 24-36 hours. Upon polymerization of the liquid in the device, the open ports were sealed with an epoxy. In the second approach, Poly(methylmethacrylate) was dissolved in the ionic liquid: 1-butyl-1-methyl pyrrolidinium bis(trifluoromethylsulfonyl)imide (in terms of wt. %, 15-25 %) by continuous stirring at 50-60 °C for eight to ten hours till a clear homogeneous transparent gel was obtained. An open faced cavity was fabricated on the PEDOT or WO<sub>3</sub> electrode using an adhesive acrylic tape and it was filled with the gel electrolyte, and heated in the oven at 60 °C, till a bubble free electrolyte was obtained. The counter electrode (PB) was then fixed onto this electrode and the whole configuration was held in place with binder clips. The device was sealed along the entire periphery of the device using epoxy and cured at room temperature. The devices based on *in-situ* polymerized gel have been designated as WO<sub>3</sub>-PB (MMA) and PEDOT-PB (MMA) and the devices prepared by direct application of the polymeric gel electrolyte were named as WO<sub>3</sub>-PB (PMMA) and PEDOT-PB (PMMA) devices.

#### 2.4. Characterization Techniques

The optical density of devices for coloration efficiency calculations was measured *in-situ*, on a Shimadzu UV-Visible-NIR 3600 spectrophotometer under dc potentials of different magnitudes (applied for a 90 s duration). Specular reflectance measurements under different dc potentials in the visible region (applied for 90 s each) were carried out in a standard mirror/device assembly using a MR 19-1 specular reflection accessory on a T90+ UV-Vis spectrophotometer. All measurements were performed with respect to a control device, devoid of any electrochromic coating, but containing the polymer (PMMA or MMA based) electrolyte, and the conducting glass substrates. The electrochemical charges intercalated / deintercalated during redox switching of the devices were determined by chronoamperometry. Cyclic voltammetry (CV) was performed for the devices with PEDOT or WO<sub>3</sub> as the working electrode and PB as the auxiliary electrode, in a two-electrode configuration (the reference was shorted with the counter electrode during the measurement) (Figure S1, supplementary information). The electrochemical potential stability window (measured by CV) and optical transmittance versus wavelength for the polymer electrolytes are shown in Figure S2 (supplementary information). All electrochemical measurements and electropolymerization were performed on an Autolab PGSTAT 302N coupled with a NOVA 1.6 software. Electrochromic switching response of the devices was performed under square wave potentials, at a fixed monochromatic wavelength, at a constant frequency, using Shimadzu UV-Visible-NIR 3600 spectrophotometer, in kinetic mode. Switching of the films was also measured on Avantes (Avaspec-2048) coupled with Autolab, in spectroelectrochemical mode in a quartz cell; the instrument was capable of scanning wavelengths from 400 to 800 nm in 1 ms. Electrochemical impedance spectroscopy was performed on the devices in the frequency range of 0.05 Hz to 10<sup>6</sup> Hz by superposition of an ac voltage of 10 mV over a zero dc potential. A thin layer of the film (WO<sub>3</sub> or PEDOT or PB) was carefully extracted using forceps in deionized water and then transferred onto a carbon coated



copper grid, 3.05 mm in diameter, and the solvent was evaporated at room temperature. A high resolution transmission electron microscope (HRTEM) FEI Tecnai G2 F 30 STWIN with a FEG source operating at 300 kV was used for structural analysis. Surface roughness of the films was measured using a Nanosurf Easy Scan atomic force microscope. X-ray diffraction (XRD) patterns were recorded on a XRD, PANalytical, X'PertPRO instrument with Cu K $\alpha$  ( $\lambda = 1.5406$  Å) radiation. For all device characterization, device dimensions of  $\sim 3$  cm  $\times$  3 cm were employed, unless mentioned otherwise, owing to constraints posed by the sample compartment dimensions for different studies.

### 3. Results and Discussion

#### 3.1. Spectroelectrochemistry of WO<sub>3</sub>-PB devices

A schematic illustrating the differences in fabrication of MMA and PMMA based devices is shown in Figures 1a and b. For fabricating the MMA based devices, the injection filled technique was used. Two open ports of about 2 mm each were created on the spacer strip affixed on a Prussian blue film (Figure 1c) and the red adhesive tape was removed as shown in the figure. The PEDOT or the WO<sub>3</sub> coated glass substrate, with the electroactive layer facing inwards was placed on the acrylic tape and allowed to cure. The MMA electrolyte in liquid state was then injected through one of the open ports, using a syringe and then the whole device assembly was heated for *in-situ* thermal polymerization. Upon solidification of the electrolyte, the two ports were sealed with an epoxy and ready for use. For synthesizing PMMA based devices, the spacer was applied along all the four edges of the Prussian blue film, without leaving any gaps (Figure 1d). The PMMA based gel electrolyte was filled in the cavity carefully with a glass rod, and the assembly was heated till a bubble free electrolyte layer was obtained (Figure 1d). At this juncture, the red overlying tape was removed and the complementary electrochromic film (PEDOT or WO<sub>3</sub>) was placed on this assembly. Upon room temperature curing, the devices were sealed with epoxy prior to use. Both MMA and PMMA based gels have hardly any flow

properties at room temperature, as can be seen from their photographs shown in Figures 1c and d. The gels do not flow even when the vials are turned upside-down.

The *in-situ* absorbance spectra of WO<sub>3</sub>-PB (MMA) and WO<sub>3</sub>-PB (PMMA) devices measured under different oxidation potentials (applied to WO<sub>3</sub>) of +0.5 to +1.5 V and reduction potentials of -0.5 to -3.5 V (in steps of 0.5 V) are shown in Figure 2a and b respectively. All  $\Delta OD_{\max}$  for the devices were determined from the difference between fully colored and bleached states and these are summarized in Table 1. As can be seen from Table 1, the WO<sub>3</sub>-PB (MMA) device shows a much larger absorbance change ( $\Delta OD_{(\max)}$ ) in contrast to the WO<sub>3</sub>-PB (PMMA) device, at all wavelengths extending even to NIR region, upto 1700 nm. For instance, a  $\Delta OD_{1060(\max)} = 1.75$  was achieved for the WO<sub>3</sub>-PB (MMA) device in comparison to a  $\Delta OD_{1060(\max)}$  of 0.62 obtained for the WO<sub>3</sub>-PB (PMMA) device. Coloration efficiencies of the devices at monochromatic wavelengths of 550, 633 and 1060 nm were deduced from the appropriate linear fits from the  $\Delta OD$  versus charge density plots which, are shown in Figures 2c and d and are also listed in Table 1.

Coloration efficiency (CE or  $\eta$ ) which, is defined as the optical density change ( $\Delta OD$ ) induced as a function of the injected electronic charge per unit area to produce the optical change is given by

$$\eta(\lambda) = \Delta OD(\lambda) / Q/A \quad (1) \text{ or by}$$

$$\eta(\lambda) = \log(T_b(\lambda)) / \log(T_c(\lambda)) / Q/A \quad (2)$$

where  $\eta$  (cm<sup>2</sup> C<sup>-1</sup>) is the coloration efficiency at a given wavelength, T<sub>b</sub> and T<sub>c</sub> are transmission in bleached and colored states at a given wavelength.<sup>4</sup> The coloration efficiency for the WO<sub>3</sub>-PB (MMA) based device was 119 cm<sup>2</sup> C<sup>-1</sup> at a photopic wavelength of 550 nm (the wavelength at which the human eye is most responsive) as compared to a value of only 54 cm<sup>2</sup> C<sup>-1</sup> at the same wavelength for the WO<sub>3</sub>-PB (PMMA) based device. The MMA based device continued to show much higher coloration efficiencies at other wavelengths as well (Table 1). On examining the

data of a Poly(aniline)-polyhedral oligomeric silsesquioxane/WO<sub>3</sub> device, we found that it showed a CE of 84 cm<sup>2</sup> C<sup>-1</sup> ( $\lambda_{\text{max}} = 625$  nm) and a  $\Delta\text{OD}$  of  $\sim 0.7$  under a potential switch of  $\pm 2$  V.<sup>9</sup> In another recent report, for a WO<sub>3</sub> film deposited on a PET (poly(ethylene terephthalate)) electrode of carbon nanotubes, a  $\Delta\text{OD}$  of 1.7 and a coloration efficiency of 64 cm<sup>2</sup> C<sup>-1</sup> was achieved in a liquid electrolyte of LiClO<sub>4</sub> in PC.<sup>28</sup> Our values are superior to the reported values of  $\Delta\text{OD}$  and CE.

Photographs of WO<sub>3</sub>-PB (MMA) devices of  $\sim 4$  cm  $\times$  10 cm dimensions are shown in bleached and colored states in Figure 2e and f. The high uniformity of colored state across the device is apparent, indicating that the device is most suitable for electrochromic window applications. The MMA based device shows larger CE values than the PMMA based one, as in the former device the electrolyte is injected in liquid state and therefore, it can easily percolate through the pores of WO<sub>3</sub> film, and subsequent to the solidification of the electrolyte by *in-situ* thermal polymerization two possibilities exist. An intimate contact is established between the WO<sub>3</sub> electrode and polymer electrolyte which, facilitates ion transfer at the electrode/electrolyte interface and secondly, a greater number of electrolyte ions can access the film, thus leading to a higher contrast and an enhanced coloration efficiency (as shown in the schematic of Figure 1a). Once the electrolyte is adsorbed, upon application of reduction potential, the three, four and six coordinated voids provided by the hexagonal structure of WO<sub>3</sub><sup>4,29</sup> can easily entrap the cations from the electrolyte. We ascertained the presence of hexagonal channels in WO<sub>3</sub> films, by high resolution transmission electron microscopy (HRTEM), which is discussed in the following section.

### 3.2. HRTEM of Electrochromic Films

The TEM image of WO<sub>3</sub> film shows a pine-tree like morphology and these long shapes with tapered ends are interconnected and uniformly distributed across the film (Figure 3a). Such a pine-tree like structure has been observed for W<sub>18</sub>O<sub>49</sub> by heating WS<sub>2</sub> in oxygen.<sup>30</sup> The high

magnification image shown in the inset of Figure 3a shows these elongated fiber like shapes to be composed of  $\text{WO}_3$  grains of no particular shape, typical of  $\text{WO}_3$  films deposited by surfactant mediated electrodeposition.<sup>31</sup> The HRTEM image of the same film shown in Figure 3b, reveals lattice fringes of  $\text{WO}_3$  with an inter-planar spacings of 0.32 and 0.39 nm which, matches well with the hexagonal crystalline structure of  $\text{WO}_3$ , as per JCPDS card number 33-1387. The d-lines correspond to (200) and (001) reflections of hexagonal  $\text{WO}_3$ . The Inverse Fast Fourier Transform (IFFT) imaging process was performed to filter out the noise in the real space HRTEM image and the enhanced lattice image was reproduced and it is shown as an inset of Figure 3b. The lattice fringes in this inset are extremely sharp and an atomic scale resolution could be achieved. The fringe spacing is 0.31 nm and it corresponds to the (200) plane of hexagonal  $\text{WO}_3$  in accordance with the JCPDS card number 33-1387. There are hardly any dislocations or defects indicating the high crystalline quality of  $\text{WO}_3$  grains. This was also confirmed from the XRD pattern which showed a preferred orientation for hexagonal  $\text{WO}_3$  along the (200) plane (Figure S3, supplementary information). Fast Fourier Transformation (FFT) was also performed and the resulting electron diffraction pattern is shown as an inset of Figure 3b. Bright spots conforming to a hexagonal crystal structure of  $\text{WO}_3$  are observed which, agrees well with the lattice scale image. Hexagonal  $\text{WO}_3$  has octahedral and tetrahedral voids which, can act as channels for ion-insertion and extraction during coloration and bleaching.<sup>4,29</sup> The bright field image of a PB film shown in Figure 3c, reveals the presence of well-connected large aggregates and the electron diffraction pattern generated by FFT (inset of Figure 3c) shows the presence of bright spots superimposed on diffuse rings. PB has a face centered cubic crystalline structure and the white spots originate from this crystal phase. The TEM image of PEDOT film (Figure 3d) shows aggregates of polymer particles and the diffraction pattern produced by FFT, shows broad and diffuse rings characteristic of the amorphous nature of the polymer.<sup>32</sup> The three dimensional AFM images of the three films are shown in Figure 3(e-g). The  $\text{WO}_3$  nodules are more

compactly packed as compared to PEDOT or PB and the WO<sub>3</sub> films have a relatively smoother texture in comparison to PEDOT or PB. This is also reflected in the significantly lower root mean square surface roughness of 1.3 nm as compared to values of 24.6 nm and 28.3 nm obtained for PB and PEDOT films respectively. A moderately high value of surface roughness enhances the electrolyte adsorption capacity of the film which, can result in higher contrast ratios.

### 3.3. Spectral Response of PEDOT-PB devices

The absorbance variation and coloration efficiency plots as a function of wavelength and applied potential for PEDOT-PB (MMA) and PEDOT-PB (PMMA) devices are shown in Figures 4 and 5. Unlike the WO<sub>3</sub>-PB (MMA) device, the PEDOT-PB (MMA) device remains slightly blue even in the bleached state (Figure 4b) due to the highly absorptive nature of oxidized PEDOT in the visible region. A maximum absorbance change of 1.27 was registered for the MMA based device at a  $\lambda_{\text{max}}$  of 600 nm (Figure 4a). The broad absorption in the NIR region in the oxidized form of PEDOT is due to the bipolaronic transitions which, loses intensity at the expense of  $\pi$ - $\pi^*$  transition peak (at 600 nm) with increasing reduction potential. Photographs of the PEDOT-PB (MMA) device of  $\sim 3 \text{ cm} \times 5 \text{ cm}$  dimensions in dark blue, and pale blue states are shown in Figure 4b. PEDOT based devices could not be up-scaled to the dimensions of WO<sub>3</sub> based ones, as on increasing the area of deposition, a high degree of non-uniformity was observed.

A similar trend for OD variation was observed for the PEDOT-PB (PMMA) device. A  $\Delta\text{OD}_{\text{max}}$  of 1.79 (with +1.5 V as the reference potential) was achieved at  $\lambda_{\text{max}}$  of 610 nm (Figure 5). In a manner, similar to the WO<sub>3</sub>-PB devices, the PEDOT-PB devices also retained a large optical change in the NIR region. Coloration efficiency plots for the PEDOT-PB (MMA) device as a function of wavelength and at different reduction potentials are shown in Figure 4c and d and the values are listed in Table 2. The reference potential was chosen as +1.5 V for the

calculations. A coloration efficiency maximum of  $287 \text{ cm}^2 \text{ C}^{-1}$  was registered for this device at a  $\lambda_{\text{max}}$  of 567 nm, under a fairly low reduction potential of  $-0.7 \text{ V}$  which, is most advantageous for maximizing the operation lifetime of the device. In the past, for a Poly(propylenedioxythiophene)-(Et)<sub>2</sub>/PB device, an unusually high coloring efficiency of  $1214 \text{ cm}^2 \text{ C}^{-1}$  was obtained.<sup>33</sup> In another study on a PEDOT/In<sub>2</sub>O<sub>3</sub>:Sn/PET film, a coloration efficiency of  $124 \text{ cm}^2 \text{ C}^{-1}$  and a  $\Delta\text{OD}$  of  $\sim 0.26$  was observed at 540 nm.<sup>28</sup> However, in both these reports, the values were achieved in a liquid electrolyte: LiClO<sub>4</sub>/PC (propylene carbonate). In another report, for a PEDOT/Gel/PB device, prepared using PET substrates, with a gel containing Li(CF<sub>3</sub>SO<sub>2</sub>)<sub>2</sub>N, 1-butyl-3-methyl imidazolium imide and PMMA, a CE of  $335 \text{ cm}^2 \text{ C}^{-1}$  was attained and a  $\Delta\text{OD}$  of  $\sim 0.77$  was observed.<sup>23</sup> The CE plot for the PEDOT-PB (PMMA) device in Figure 5b shows this device to have a  $\text{CE}_{\text{max}}$  of  $267 \text{ cm}^2 \text{ C}^{-1}$  at  $\sim 695 \text{ nm}$  (under  $E = -1.5 \text{ V}$ ). CE values were lower at other potentials. It is obvious that the PMMA based device requires a higher potential ( $E = -1.5 \text{ V}$ ) to acquire a  $\text{CE}_{\text{max}}$ , whereas an external bias of only  $-0.7 \text{ V}$ , was sufficient for reaching a higher value of  $\text{CE}_{\text{max}}$  in its MMA counterpart. A lesser amount of charge suffices to generate a greater electrochromic efficiency in the MMA based device which, is beneficial for prolonging the functional lifetime of the device. We must mention that the CE plots for the PMMA based devices for  $E > 1.5 \text{ V}$  are not shown here, and the wavelength range was limited to a maximum of 1000 nm, in comparison to a limit of 1600 nm for the MMA based device, as the curves for the PMMA were noisy, possibly due to increased scattering of radiation by the electrolyte under high potentials.

The specular reflectance variation as a function of wavelength in the visible region of the devices was measured under oxidation and reduction potentials within the range of  $+2.5 \text{ V}$  to  $-3.5 \text{ V}$  (Figure 6). The PEDOT-PB (PMMA) device showed extremely small changes in reflectance with potential, (Figure S4, supplementary information), due to low transparency even in the oxidized state. Permanent pyrrolidinium ion entrapment in the electrodes which, results in

irreversible coloration could be responsible for the poor reflectance modulation ( $\Delta R$ ). The  $\Delta R_{\max}$  values are listed in Table S1 (supplementary information). Again, the  $\text{WO}_3$ -PB (MMA) and the PEDOT-PB (MMA) devices showed higher values of  $\Delta R_{\max}$  as compared to their PMMA counterparts (Table S1). Although the magnitude of reflectance modulation is lower than the corresponding absorptive modulation of these devices, nevertheless  $\Delta R$  values are reasonably high for their application to reflective electrochromic devices. The superiority of electrolyte filling by injection and *in-situ* thermal polymerization method is obvious. Our values are comparable to values reported in literature for devices of smaller dimensions. Earlier, for a PEDOT based device, a reflectance contrast of 40% was achieved at a photopic wavelength of 573 nm for 95 % of the full switch.<sup>6</sup>

#### 3.4. Switching Kinetics

Coloration - bleaching characteristics of PEDOT-PB (MMA) and  $\text{WO}_3$ -PB (MMA) devices recorded at monochromatic wavelengths ( $\lambda_{\max}$ ) of 585 and 685 nm, with 3 and 5 s as step times, under a square wave potential of  $\pm 2.0$  V, are shown in Figure 7. The time required for absorbance to increase from 10% to 90% of its full switch in a half cycle is coloration time and for absorbance to decrease from 90% to 10% of its total magnitude is the bleaching time. Under a step time of 3 s (Figure 7a) a coloration time of 2.0 s and a bleaching time of 2.2 s was observed for the PEDOT-PB (MMA) device. For the  $\text{WO}_3$ -PB (MMA) device (Figure 7b), color time was 2.1 s and bleach time was 1.7 s (half cycle time is 3 s). Coloration kinetics is faster than bleaching for the PEDOT based device, whereas bleaching is faster than coloration for the  $\text{WO}_3$  based device. Since in the bleaching cycle, the back *emf* opposes the applied potential, the diffusion of the cations from the  $\text{WO}_3$  film is hindered as the pyrrolidinium ion is a bulky organic molecule and as a result bleaching takes longer time. Also in oxides, the film morphology is known to affect bleaching more than coloration and therefore the hexagonal structure of  $\text{WO}_3$ , allows faster de-intercalation. In the PEDOT based devices, it is the anion

insertion and extraction from the polymer film which, controls switching rates. Coloration is faster here, as imide ion extraction is facilitated by the large separation between polymer chains caused by the expansion of the molecular network, upon incorporation of camphorsulfonate counterions used during oxidative electropolymerization of EDOT. Coloration of PEDOT is also accompanied by the transition from the conducting doped state to the neutral state, the ease of electron injection into the matrix of a not yet insulating film promotes faster color kinetics. Color and bleach times of 13 s and 5 s were achieved for a  $\text{WO}_3$  nanorod film, in a  $\text{LiClO}_4/\text{PC}$  solution under applied potentials of  $\pm 3 \text{ V}^{34}$  and for a PANI- $\text{WO}_3$  device, a coloring time of  $\sim 17 \text{ s}$  was registered.<sup>9</sup> The PMMA based devices showed slower kinetics and a smaller magnitude of optical density change (Figure S5, supplementary information) for the same values of applied potential as used for the MMA based devices. Moderately fast switching kinetics shown by MMA based devices renders them suitable for smart window applications. To further confirm that absorbance in the visible region indeed changes rapidly in PEDOT film, the dynamic change in absorbance was measured during redox switching. The films were subjected to an oxidation potential of +1.0 V for 3 s and the dynamic absorbance, wherein the instrument scans 300-800 nm wavelength range within 1 ms was measured. In a similar manner, dynamic spectral responses of the same film were recorded under a reduction potential of -1.0 V for durations of 10, 15, 20, 25 and 30 s (Figure 8). The film acquires a saturated blue color within 25 s, as the dynamic response measured for a 30 s duration re-traces the curve obtained in the 25 s cycle. From the curves it is obvious, that the film acquires  $\sim 69\%$  of the total absorption change that it is capable of attaining, within 5 s. This is a clear indicator of the fact that film shows fast kinetics. Bleaching is also fast, as the peak due to  $\pi\text{-}\pi^*$  absorption vanishes in a span of 3 s.

### 3.5. Electrochemical Impedance Spectroscopy

Nyquist plots of  $\text{WO}_3\text{-PB}$  (MMA),  $\text{WO}_3\text{-PB}$  (PMMA), PEDOT-PB (MMA) and PEDOT-PB (MMA) devices are shown in Figure 9(a-d) and Bode plots are shown in the corresponding



insets. The equivalent circuit displayed in Figure 9a was found to give excellent fits for all  $Z''$  versus  $Z'$  curves and the fitted/calculated parameters are summarized in Table S2 (supplementary information). The PEDOT-PB (MMA) device shows an arc in the high frequency region, whereas only a slight curvature is observed for the PEDOT-PB (PMMA) device. For the  $\text{WO}_3$ -PB devices, a nearly straight line behavior is observed which is characteristic of fast charge transfer at the  $\text{SnO}_2\text{:F}/\text{WO}_3$ ,  $\text{WO}_3/\text{electrolyte}$  interfaces and also of rapid ion transport through the bulk of the  $\text{WO}_3$  film. As can be seen from the Bode plots, the magnitude of impedance ( $|Z|$ ) is larger for the MMA based devices, in comparison to the PMMA based devices. Ionic conductivities of the two electrolytes were determined from the impedance plots and for the MMA based gel, it is  $1.6 \times 10^{-4} \text{ S cm}^{-1}$ . The PMMA based gel shows an ionic conductivity of  $4.2 \times 10^{-5} \text{ S cm}^{-1}$ . In the past, a poly(ethyl methacrylate)- $\text{LiClO}_4/\text{PC}$  based electrolyte, showed a room temperature ionic conductivity of  $6.9 \times 10^{-4} \text{ S cm}^{-1}$ <sup>14</sup> and a dried polyelectrolyte film of poly(ethylene imine)/poly(acrylic acid)/ $\text{LiCF}_3\text{SO}_3$ , prepared by layer-by-layer assembly method was characterized by an ionic conductivity greater than  $10^{-5} \text{ S cm}^{-1}$  at ambient temperature.<sup>16</sup> The charge transfer resistances ( $R_{CT}$ ) for the MMA based devices are smaller in magnitude as compared to the PMMA based devices (Table S2). It is apparent that the MMA based electrolyte forms a more intimate contact with the electrode (PEDOT or  $\text{WO}_3$ ) surface as it is introduced in the device in a liquid state in contrast to the PMMA based electrolyte which, is incorporated in a semi-solid state and therefore does not attach to the electrode as effectively as the MMA electrolyte does. This inference is also supported by the fact that both exchange current density and diffusional pseudocapacitance (the measure of charging in the bulk of the film in the low frequency region) have larger values for the MMA based devices in contrast to the PMMA based devices (Table S2).

#### 4. Conclusions

Two methods were used for synthesizing and applying polymer electrolytes to electrochromic devices of WO<sub>3</sub>-PB and PEDOT-PB. In the first approach, a homogeneous transparent gel formed by immobilization of PMMA in an ionic liquid was applied to the devices whereas in the second method, direct *in-situ* thermal polymerization of the monomer in the devices was performed after injecting the MMA-ionic liquid solution in the devices. The *in-situ* polymerized gel, by the virtue of being introduced into the device in a liquid state, allows the formation of better interfacial contacts which, reduces the charge transfer resistance and thus enables faster intercalation-deintercalation reactions at the electrochromic electrode. It also allows a greater number of electrolyte ions to access the redox active sites in the electrochromic films which, results in high contrast, thus resulting in a coloring efficiency of 119 cm<sup>2</sup> C<sup>-1</sup> ( $\lambda_{\max}$  = 550 nm) for the WO<sub>3</sub>-PB (MMA) based device as compared to a CE of 54 cm<sup>2</sup> C<sup>-1</sup> at the same wavelength for the WO<sub>3</sub>-PB (PMMA) based device. The role of film microstructure was found to affect ion insertion-extraction kinetics and therefore the open channels provided by the four/six/three coordinated voids created by the the hexagonal crystal structure of the WO<sub>3</sub> film impacted bleaching kinetics favorably. Devices prepared by direct incorporation of the gel electrolyte, do not have either of the above mentioned two advantages and therefore the electrochromic performance is adversely affected. Large area devices were successfully fabricated using the *in-situ* polymerized gel and their ability to color uniformly without any pinholes or color gradients, indicates the promise this method holds for upscaling it further and application to commercial electrochromic devices.

### **Acknowledgements**

Financial support from Department of Science & Technology (DST/TSG/PT/2007/69) is gratefully acknowledged. One of the authors, Rambabu Sydam acknowledges DST and University Grants Commission for junior research fellowship.

### **Electronic Supplementary Information**

Supplementary data associated with this article can be found in the online version at doi.xxx.

## References

- 1 D. T. Gillaspie, R. C. Tenent and A. C. Dillon, *J. Mater. Chem.*, 2010, **20**, 9585.
- 2 S. V. Vasilyeva, P. M. Beaujuge, S. Wang, J. E. Babiarz, V. W. Ballarotto and J. R. Reynolds, *ACS Appl. Mater. Interfaces*, 2011, **3**, 1022.
- 3 G. A. Niklasson and C. G. Granqvist, *J. Mater. Chem.*, 2007, **17**, 127.
- 4 C. G. Granqvist, *Handbook of Inorganic Electrochromic Materials*, Elsevier: Amsterdam, 1995.
- 5 P. M. S. Monk, R. J. Mortimer and D. R. Rosseinsky, *Electrochromism and Electrochromic Devices*, Cambridge University Press: United Kingdom, 2007.
- 6 P. -H. Aubert, A. A. Argun, A. Cirpan, D. B. Tanner and J. R. Reynolds, *Chem. Mater.*, 2004, **16**, 2386.
- 7 C. S. Blackman and I. P. Parkin, *Chem. Mater.*, 2005, **17**, 1583.
- 8 S. Kirchmeyer and K. Reuter, *J. Mater. Chem.*, 2005, **15**, 2077.
- 9 L. Zhang, S. Xiong, J. Ma and X. Lu, *Sol. Energy Mater. Sol. Cells*, 2009, **93**, 625.
- 10 A. A. Argun, A. Cirpan and J. R. Reynolds, *Adv. Mater.*, 2003, **15**, 1338.
- 11 A. Kumar, D. M. Welsh, M. C. Morvant, F. Piroux, K. A. Abboud and J. R. Reynolds, *Chem. Mater.*, 1998, **10**, 896.
- 12 R. J. Mortimer and J. R. Reynolds, *J. Mater. Chem.*, 2005, **15**, 2226.
- 13 C. A. Nguyen, S. Xiong, J. Ma, X. Lu and P. S. Lee, *J. Phys. Chem. B*, 2009, **113**, 8006.
- 14 J. Reiter, O. Krejza and M. Sedlarkova, *Sol. Energy Mater. Sol. Cells*, 2009, **93**, 249.
- 15 E. D. C. Rios, A. V. Rosario, A. F. Nogueira and L. Micaroni, *Sol. Energy Mater. Sol. Cells*, 2010, **94**, 1338.
- 16 C. A. Nguyen, A. A. Argun, P. T. Hammond, X. Lu and P. S. Lee, *Chem. Mater.*, 2011, **23**, 2142.

- 17 J. Zhang, J. P. Tu, X. H. Xia, Y. Qiao and Y. Lu, *Sol. Energy Mater. Sol. Cells*, 2009, **93**, 1840.
- 18 C.-Y. Kim, S.-G. Cho and T. -Y. Lim, *Sol. Energy Mater. Sol. Cells*, 2009, **93**, 2056.
- 19 F. Tran-Van, L. Beouch, F. Vidal, P. Yammine, D. Teyssie and C. Chevrot, *Electrochim. Acta*, 2008, **53**, 4336.
- 20 L. Su, J. Fang, Z. Xiao and Z. Lu, *Thin Solid Films*, 1997, **306**, 133.
- 21 S. I. Cho and S. B. Lee, *Acc. Chem. Res.*, 2008, **41**, 699.
- 22 D. DeLongchamp and P. T. Hammond, *Adv. Mater.*, 2001, **13**, 1455.
- 23 S. Duluard, A. C. -Cochet, I. Saadeddin, A. Labouret, G. Campet, G. Schottner, U. Posset and M. -H. Delville, *New J. Chem.*, 2011, **35**, 2314.
- 24 M. Deepa, A. Awadhia and S. Bhandari, *Phys. Chem. Chem. Phys.*, 2009, **11**, 5674.
- 25 M. Deepa, A. Awadhia, S. Bhandari and S. L. Agrawal, *Electrochim. Acta*, 2008, **53**, 7266.
- 26 M. Dobbelin, I. Azcune, M. Bedu, A. R. de Luzuriaga, A. Genua, V. Jovanovski, G. Cabanero and I. Odriozola, *Chem. Mater.*, 2012, **24**, 1583.
- 27 T. Sato, G. Masuda and K. Takagi, *Electrochim. Acta*, 2004, **49**, 3603.
- 28 R. M. Osuna, V. Hernandez, J. T. L. Navarrete, E.I. Kauppinen and V. Ruiz, *J. Phys. Chem. Lett.*, 2010, **1**, 11367.
- 29 S. Balaji, Y. Djaoued, A. -S. Albert, R. Z. Ferguson and R. Bruning, *Chem. Mater.*, 2009, **21**, 1381.
- 30 W. B. Hu, Y. Q. Zhu, W. K. Hsu, B. H. Chang, M. Terrones, N. Grobert, H. Terrones, J. P. Hare, H. W. Kroto and D. R. M. Walton, *Appl. Phys. A*, 2000, **70**, 231.
- 31 M. Deepa, A. K. Srivastava, S. Lauterbach, Govind, S. M. Shivaprasad and K. N. Sood, *Acta Mater.*, 2007, **50**, 6095.

32 S. Bhandari, M. Deepa, S. Pahal, A. G. Joshi, A. K. Srivastava and R. Kant, *ChemSusChem*, 2010, **3**, 97.

33 K. -C. Chen, C. -Y. Hsu, C. -W. Hu and K. -C. Ho, *Sol. Energy Mater. Sol. Cells*, 2011, **95**, 2238.

34 J. Wang, E. Khoo, P. S. Lee and J. Ma, *J. Phys. Chem. C*, 2008, **112**, 14306.

## Tables

**Table 1:** Electrochromic parameters for WO<sub>3</sub>-PB devices, where  $\Delta OD_{\max} = OD(-3.5 \text{ V}) - OD(+1.5 \text{ V})$  and  $CE = \Delta OD_{\max}/Q(-3.5 \text{ V})/\text{area}$ .

Device	$\lambda$ (nm)	$\Delta OD_{\max}$ (a.u.) MMA	$\Delta OD_{\max}$ (a.u.) PMMA	CE (cm <sup>2</sup> C <sup>-1</sup> ) MMA	CE (cm <sup>2</sup> C <sup>-1</sup> ) PMMA
WO <sub>3</sub> -PB	550	0.79	0.20	119	54
WO <sub>3</sub> -PB	633	1.00	0.29	149	80
WO <sub>3</sub> -PB	1060	1.75	0.62	203	147

**Table 2:** Electrochromic parameters for PEDOT-PB devices, where  $\Delta OD = OD(-0.7 \text{ V}) - OD(+1.5 \text{ V})$  (for MMA based) and  $\Delta OD = OD(-1.5 \text{ V}) - OD(+1.5 \text{ V})$  (for PMMA based) and  $CE = \Delta OD/Q(-0.7 \text{ V or } -1.5 \text{ V})/\text{area}$ .

E for CE <sub>max</sub> (V) MMA	$\lambda$ (nm)	CE <sub>max</sub> (cm <sup>2</sup> C <sup>-1</sup> ) MMA	E for CE <sub>max</sub> (V) PMMA	$\lambda$ (nm)	CE <sub>max</sub> (cm <sup>2</sup> C <sup>-1</sup> ) PMMA
-0.7 V	567 ( $\lambda_{\max}$ )vis	287	-1.5 V	695 ( $\lambda_{\max}$ )vis	267
-0.7 V	550	283	-1.5 V	550	108
-0.7 V	633	274	-1.5 V	633	217
-0.7 V	1145 ( $\lambda_{\max}$ )NIR	706	-1.5 V	993 ( $\lambda_{\max}$ )NIR	282

## Figures

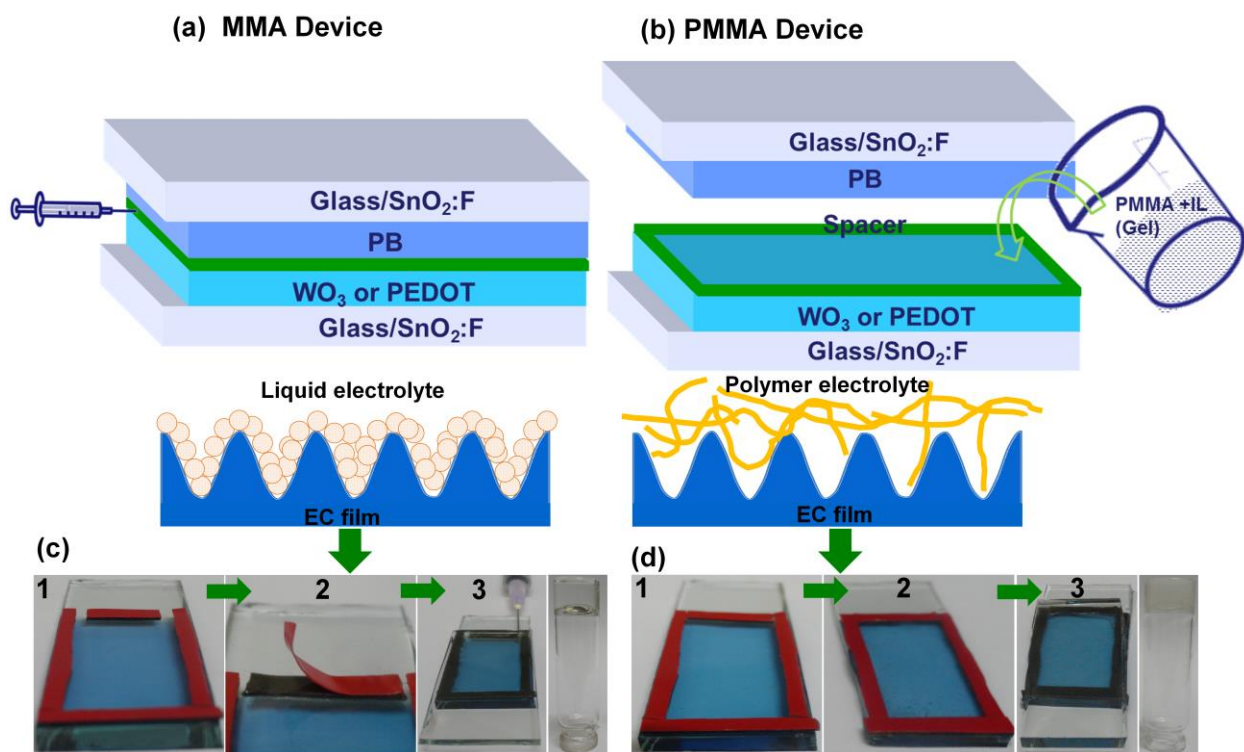


**Figure 1** Schematics of protocols used for device fabrication in (a) MMA and (b) PMMA based devices and the corresponding electrode/electrolyte interface in each case. Sequence of steps followed in fabrication of (c) MMA based devices: (1) Open ports on a PB layer with a spacer, (2) removal of adhesive tapes and (3) application of a WO<sub>3</sub> layer and injection of electrolyte and (d) PMMA based devices: (1) creation of cavity with a spacer on a PB layer, (2) Cavity filled with PMMA electrolyte and (3) removal of red adhesive tape and application of WO<sub>3</sub> layer. The inverted vials in (c) and (d) are photographs of MMA and PMMA electrolytes.

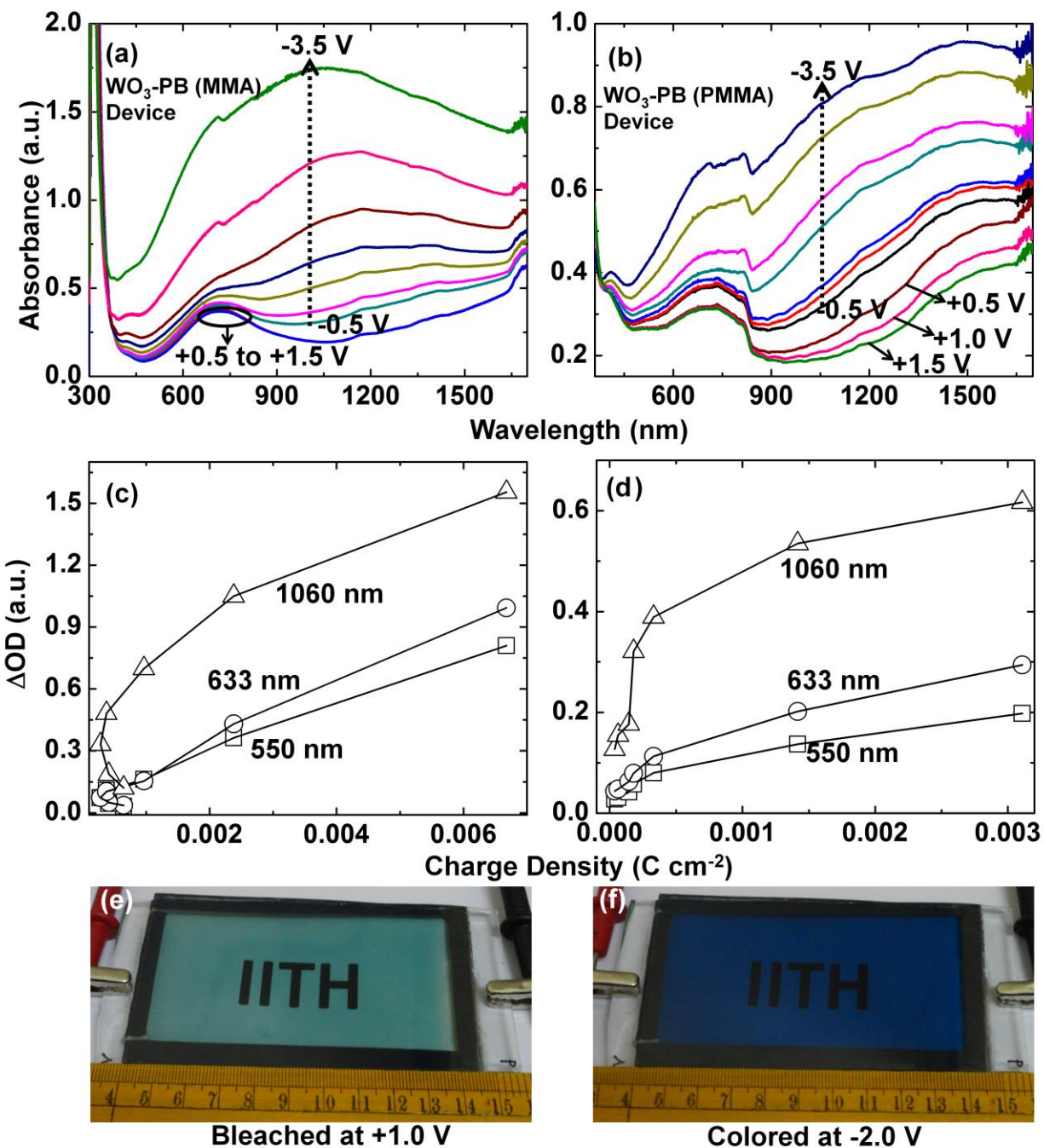


**Figure 2** *In-situ* absorbance spectra of a (a) WO<sub>3</sub>-PB (MMA) and (b) WO<sub>3</sub>-PB (PMMA) devices in the wavelength range of 350 -1700 nm recorded under oxidation potentials of +0.5, +1.0 and +1.5 V and under reduction potentials of -0.5 V to -3.5 V, in steps of 0.5 V, applied for 90 s each. Optical density change versus charge density plots of (c) WO<sub>3</sub>-PB (MMA) and (d) WO<sub>3</sub>-



PB (PMMA) devices; photographs of WO<sub>3</sub>-PB (MMA) device in (e) bleached and (f) colored states.

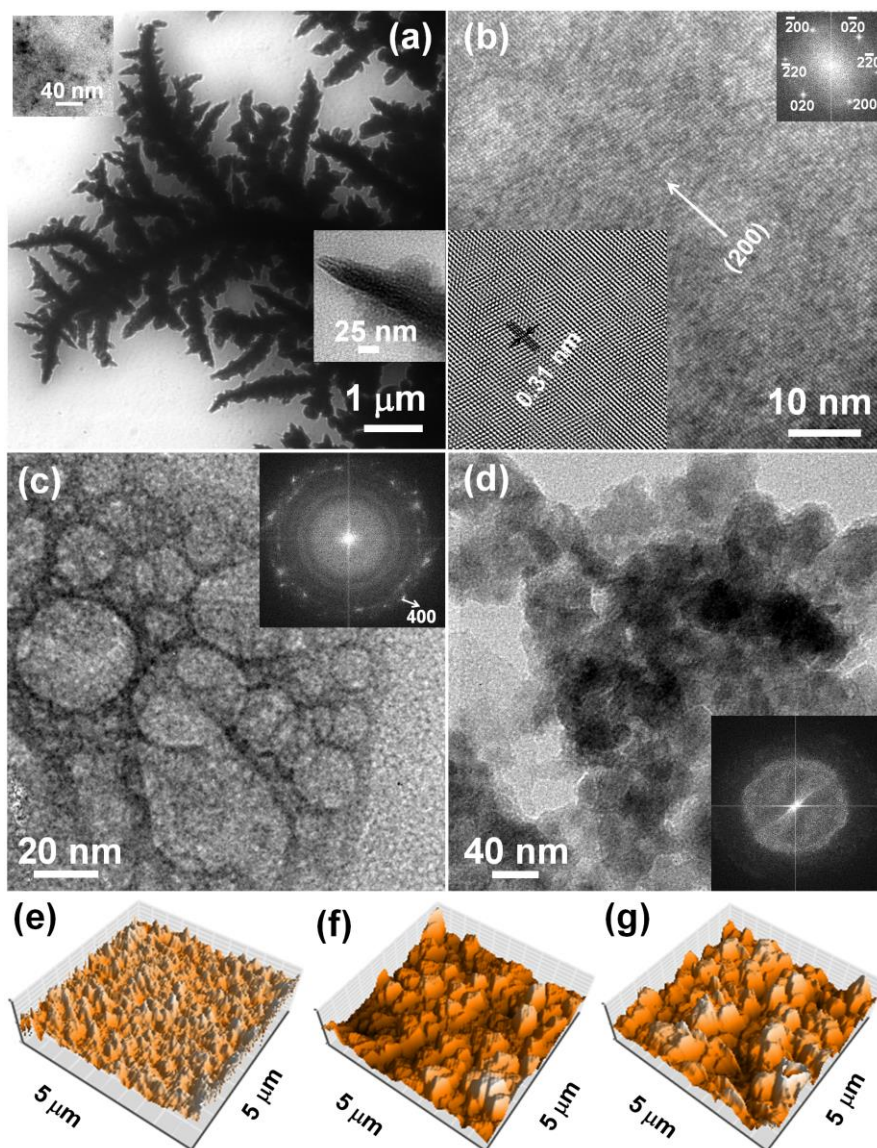


**Figure 3** (a) Bright field image of a WO<sub>3</sub> film; insets on left and right are high and low magnification images, (b) HRTEM image of WO<sub>3</sub>, inset on right is an IFFT of the same, TEM images of a (c) PB and (d) a PEDOT film, insets of b,c and d show the corresponding electron diffraction images generated by FFT. Three dimensional AFM images of (e) WO<sub>3</sub>, (f) PB and (g) PEDOT films.

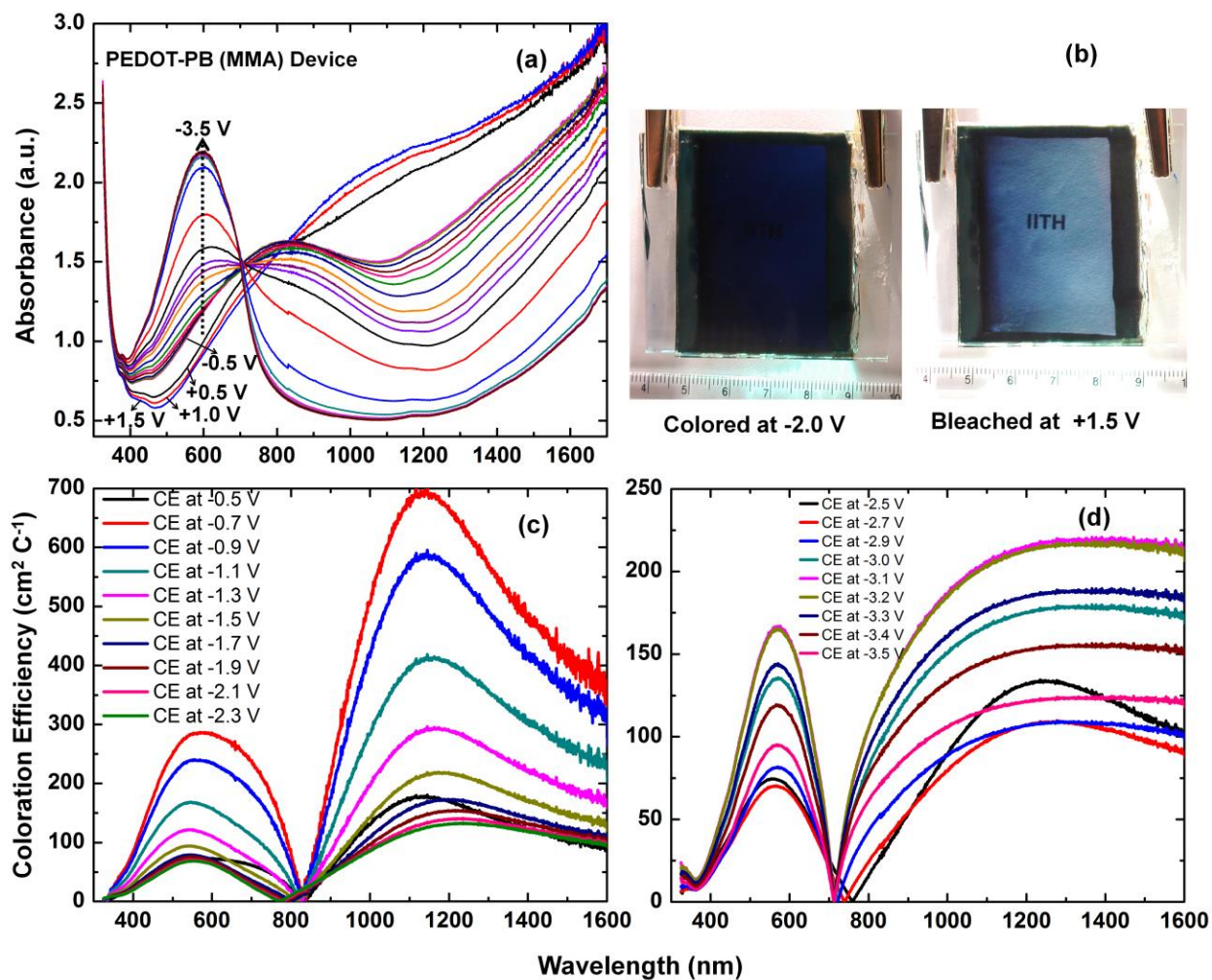


**Figure 4** (a) *In-situ* absorbance spectra of a (a) PEDOT-PB (MMA) device devices in the wavelength range of 350 -1700 nm recorded under oxidation potentials of +0.5, +1.0 and +1.5 V and under reduction potentials of -0.5 V to -2.9 V, in steps of 0.2 V and from -3.0 to -3.5 V, in steps of 0.1 V, applied for 90 s each. (b) Photographs of a PEDOT-PB (MMA) device in colored and bleached states, coloration efficiency plots of PEDOT-PB (MMA) device as a function of wavelength for reduction potentials between (c) -0.5 and -2.3 V and (d) -2.5 and -3.5 V; the optical state under +1.5 V in (a) was chosen as reference.

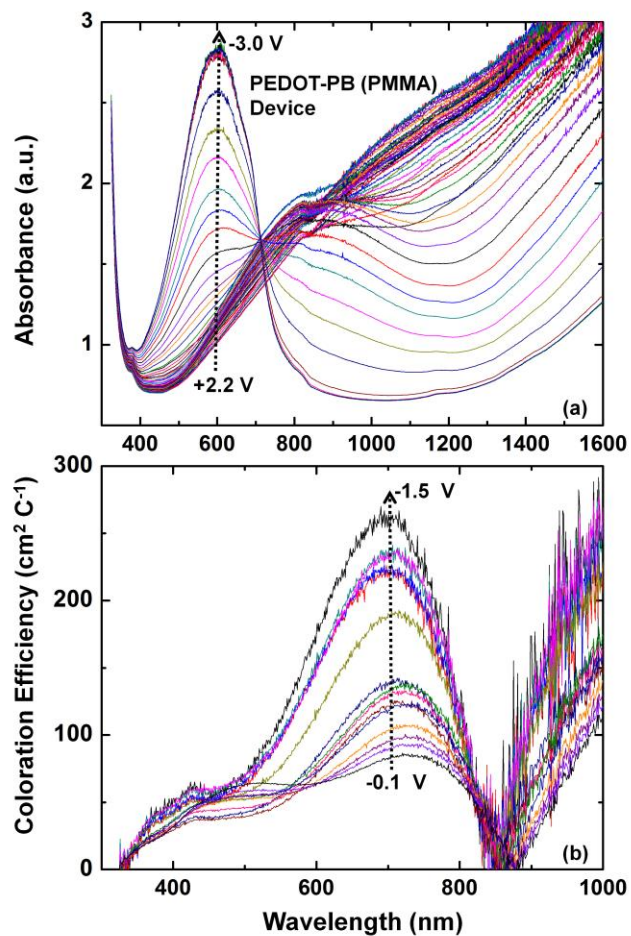


**Figure 5** (a) *In-situ* absorbance spectra of a (a) PEDOT-PB (PMMA) device recorded under potentials of +2.2 V to -3.0 V, in steps of 0.1 V, applied for 90 s each and (b) coloration efficiency of a PEDOT-PB (PMMA) device as a function of wavelength for reduction potentials between -0.1 and -1.5 V; the optical state under +1.5 V in (a) was chosen as reference.

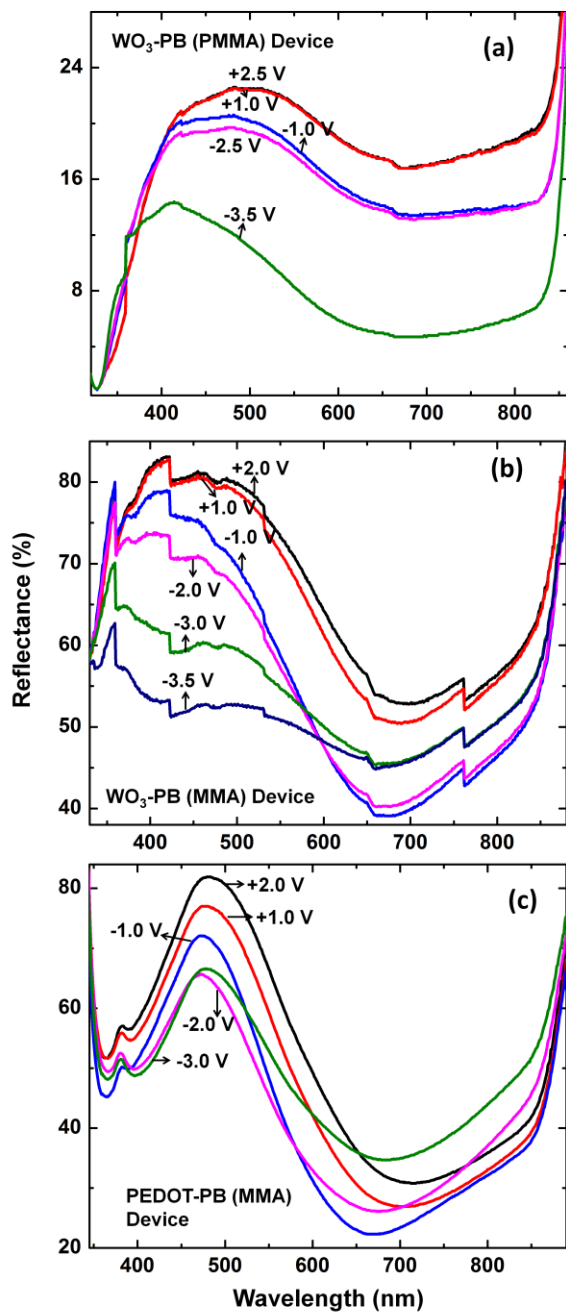


**Figure 6** *In-situ* specular reflectance of (a)  $\text{WO}_3$ -PB (PMMA), (b)  $\text{WO}_3$ -PB (MMA) and (c) PEDOT-PB (MMA) devices versus wavelength recorded with respect to a standard mirror/control device assembly under different dc potentials in the range of +2.5 V to -3.5 V.



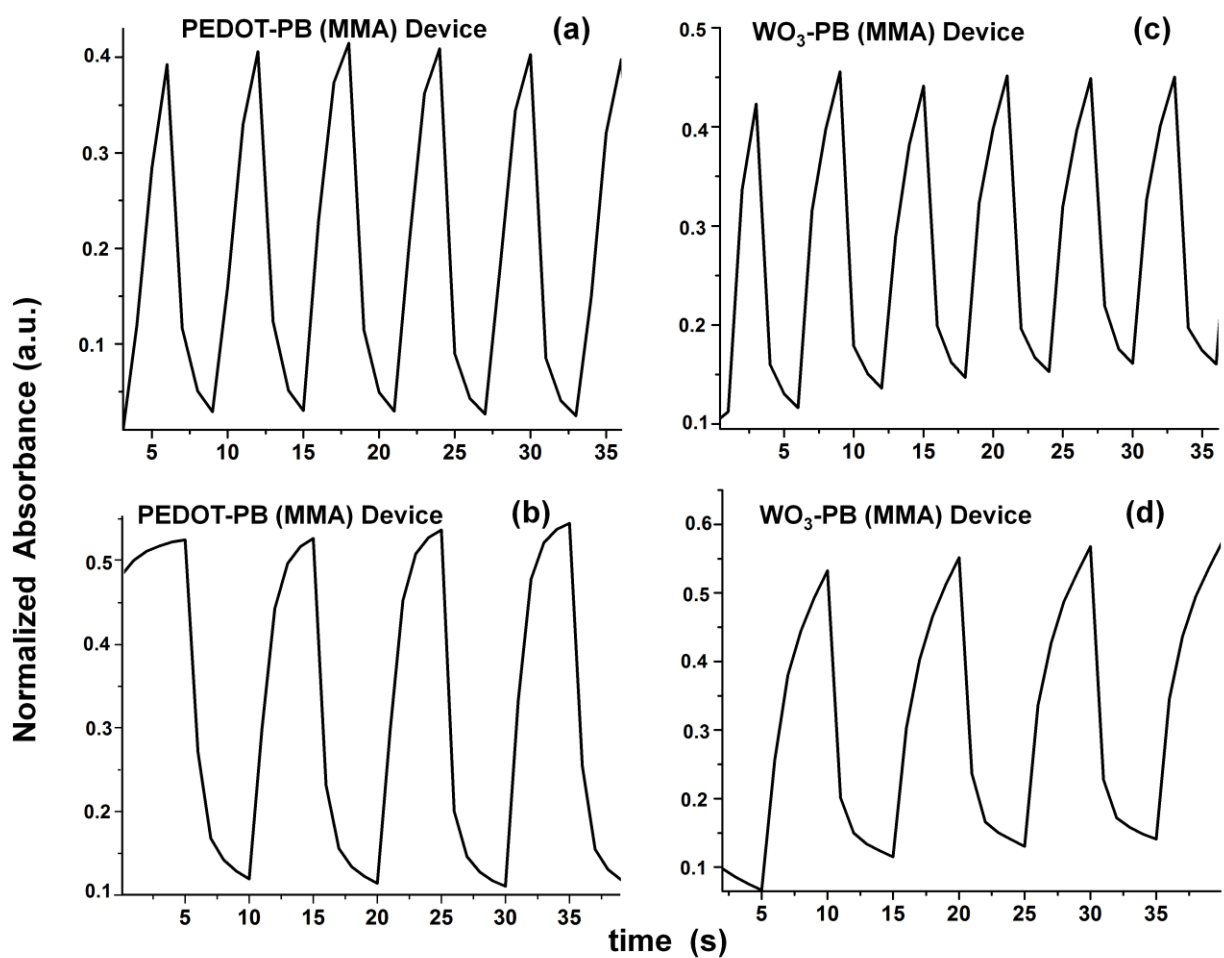


**Figure 7** Color-bleach kinetics of a PEDOT-PB (MMA) device recorded at a  $\lambda_{\max}$  of 585 nm with a step time of (a) 3 s and (b) 5 s and of WO<sub>3</sub>-PB (MMA) device at a  $\lambda_{\max}$  of 685 nm with a step time of (c) 3 s and (d) 5 s.

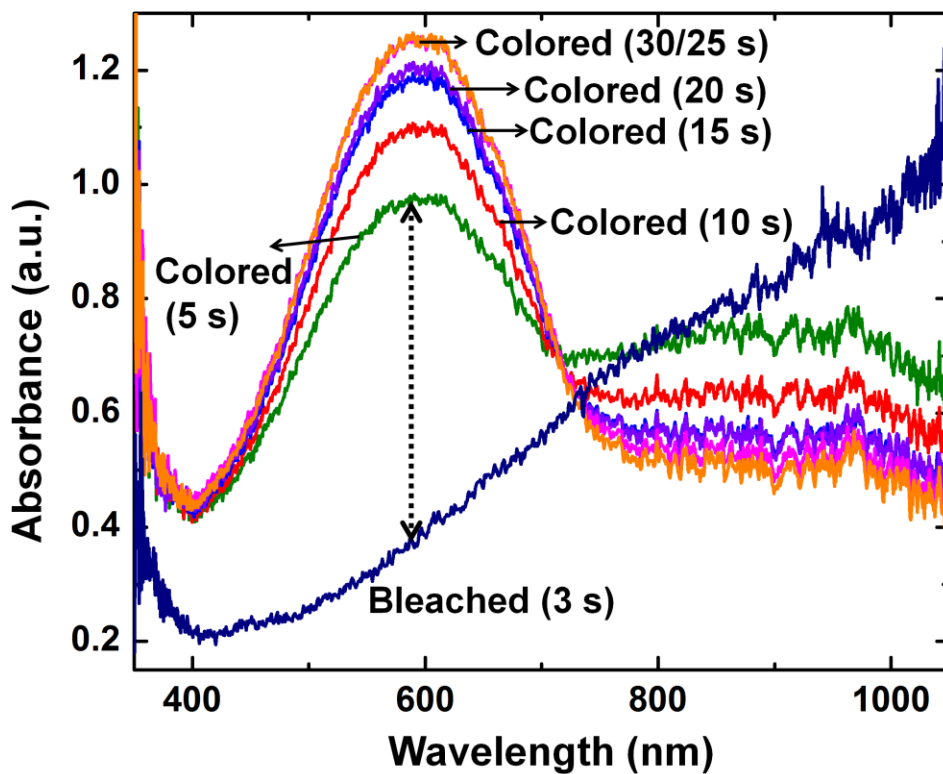


**Figure 8** Dynamic absorbance spectrum of a PEDOT film, recorded in a liquid electrolyte, wherein the wavelength range of ~400 to 800 nm is swept within 1 ms, under dc potentials of +1.0 V (for bleaching) and -1.0 V (for coloration).

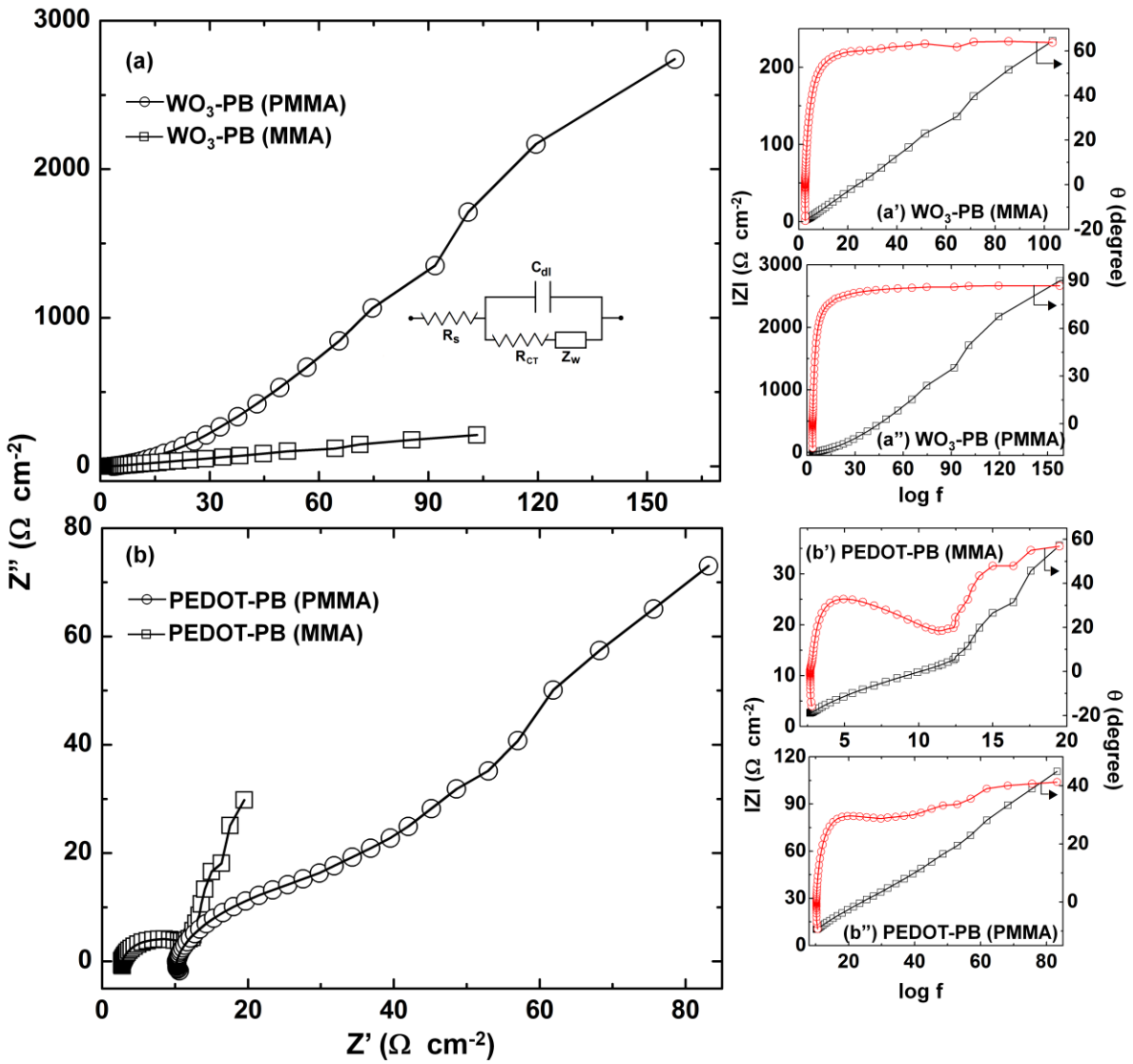


**Figure 9** Nyquist plots of (a)  $\text{WO}_3$ -PB (MMA) ( $\square$ ) and  $\text{WO}_3$ -PB (PMMA) ( $\circ$ ) devices and (b) PEDOT-PB (MMA) ( $\square$ ) and PEDOT-PB (PMMA) ( $\circ$ ) devices recorded under an ac amplitude of 10 mV; (a',a'',b',b'') are the corresponding Bode plots ( $\square$ )  $|Z|$  versus  $\log$  (frequency) and ( $\circ$ )  $\theta$  versus  $\log$  (frequency). Symbols represent the experimental data and the solid lines ( $\text{—}$ ) are obtained by fitting the experimental data in the model shown in (a).